Indication for an anomalous magnetoresistance mechanism in $(Bi, Sb)_2(Te, Se)_3$ three-dimensional topological insulator thin films

N. P. Stepina,[1,*] A. O. Bazhenov,[1] A. V. Shumilin,[2,3] A. Yu. Kuntsevich,[4] V. V. Kirienko,[1] E. S. Zhdanov,[1] D. V. Ishchenko,[1] and O. E. Tereshchenko[1]

[1]*Institute of Semiconductor Physics, 630090 Novosibirsk, Russia*
[2]*Ioffe Institute, 194021 St. Petersburg, Russia*
[3]*Jozef Stefan Institute, Ljubljana 1000, Slovenia*
[4]*P. N. Lebedev Physical Institute, Russian Academy of Sciences, 119991 Moscow, Russia*

(Received 8 April 2023; revised 30 May 2023; accepted 11 August 2023; published 5 September 2023)

Electron states with the spin-momentum-locked Dirac dispersion at the surface of a three-dimensional (3D) topological insulator are known to lead to weak antilocalization (WAL), i.e., low temperature and low-magnetic-field quantum interference-induced positive magnetoresistance (MR). In this work, we report on the MR measurements in $(Bi, Sb)_2(Te, Se)_3$ 3D topological insulator thin films epitaxially grown on Si(111), demonstrating an anomalous WAL amplitude. This anomalously high amplitude of WAL cannot be explained by parabolic or linear MR and indicates the existence of an additional MR mechanism. Another supporting observation is not linear in the classically weak magnetic field Hall effect in the same films. The increase of the low-field Hall coefficient, with respect to the higher-field value, reaches 10%. We consistently explain both transport features within a two-liquid model, where the mobility of one of the components strongly drops in a weak magnetic field. We argue that this dependence may arise from the Zeeman-field-induced gap opening mechanism.

DOI: 10.1103/PhysRevB.108.115401

I. INTRODUCTION

Magnetotransport in three-dimensional (3D) topological insulators (TIs) has been a matter of intensive investigation in recent years [1–3]. Layered 3D TIs of a tetradymite structure (Bi_2Se_3, Bi_2Te_3, and so on) are the most studied [4,5]. The conductivity of films and crystals of these materials is generally believed to consist of three channels connected in parallel: bulk and two surfaces (top and bottom). Revealing the topologically protected surface states (TSSs) requires the suppression of bulk conductivity by reducing the thickness of the film or flake. This three-channel picture has become paradigmatic. Multiple channels emerge in the transport as a positive magnetoresistance (MR) and a simultaneously nonlinear Hall effect ($\mu B \sim 1$, where μ is the mobility) and are described within two or three liquid models [6–8]. In quantum transport, the Dirac TSSs must lead to the semi-integer quantum Hall effect; however, its observation is tricky because 3D TIs have two surfaces [9]. In view of quantum transport, TSSs also lead to positive magnetoresistance with a cusplike minimum at $B = 0$ due to a weak-antilocalization (WAL) suppression by the magnetic field. An efficient number of conductivity channels directly enters the WAL amplitude, i.e., the prefactor α_{WAL} value obtained from the Hikami-Larkin-Nagaoka (HLN) fit [10] of the low-field magnetoconductivity (MC). For a single channel, α_{WAL} should be equal to -0.5, for two channels $\alpha_{\mathrm{WAL}} = -1$, correspondingly. When the bulk carriers contribute to MC, a nonzero interlayer coupling can arise; as a result, experimentally, the α_{WAL} often lies in the interval between -0.5 and -1 [11–15].

Apparently unphysical elevated values of $\alpha_{\mathrm{WAL}} > 1$ were observed in a number of papers [2,13,16–20]. For example, Ref. [16] reports $\alpha_{\mathrm{WAL}} \sim 6$. In several studies, these large α values were attributed to the classical linear [21,22] or quadratic [13,23] effects. Nevertheless, in some papers [13,16], large values of α_{WAL} persist even with these effects taken into account.

In this work, we experimentally focus on the Hall effect and MC studies in the low-field domain in $Bi_{2-x}Sb_xTe_{3-y}Se_y$ (BSTS) films, where WAL is observed. Quaternary compound BSTS were used to decrease the bulk concentration [8,9,24–26], which is high due to the doping by intrinsic point defects in binary 3D TI tetradymites, such as Bi_2Se_3 [27] and Bi_2Te_3 [6]. We reveal an elevated amplitude of the WAL and show that this enhancement cannot be attributed to the electron-electron interaction or an admixture of linear or quadratic MR, as was previously conjectured [16,22].

Naive understanding and the theory of weak localization [28,29] suggests that in the low-field limit, the Hall resistance should be linear in the magnetic field. However, we observe the opposite: the Hall coefficient may vary by as much as 10–20%.

We note that Hall nonlinearity has been previously observed in single crystals and thin films of 3D TIs and is always described in terms of the multiliquid model, i.e., the parallel connection of several conductive channels with various densities n_i and field-independent mobilities μ_i [6–8]. Within

*nstepina@mail.ru

this model, the Hall effect deviates from the linear-in-field behavior in a magnetic field, $>1/\mu_{\max}$, where $\mu_{\max}$ is the highest mobility among the components. Since the maximal mobility ever reached in thin films of bismuth chalcogenides is about 1 $m^2/Vs = 1\ T^{-1}$, one would not expect strong Hall nonlinearity below 1 T, which is the classically weak magnetic field for our films ($\mu B \ll 1$).

Small Hall effect nonlinearity in a classically low magnetic field was observed in various material systems, including 2D gases in GaAs [30], Si [31], and $LaAlO_3/SrTiO_3$ [32] doped semiconductors [33,34], and indium oxide [35]. In all cases, the effect strongly depends on the temperature and the Hall feature sharpens in the low-temperature limit. Several theoretical mechanisms were suggested, including second-order corrections [30], memory effects [36], superconducting fluctuations [37], and a combination of nonuniformity and quantum interference [38]. These theories (besides Ref. [36], which is not related to our case) also explain temperature-dependent Hall nonlinearity.

We believe, therefore, that all these mechanisms are irrelevant in our case of thin 3D TIs films. A large effect value, its elevated value in the lowest-density films, and weak temperature dependence force us to suggest that the effect is related to the (i) low-field transport current redistribution due to conductivity drop in one channel and (ii) emergence of this drop from the magnetic-field effect on the electron spectrum.

We suggest that the anomalous WAL amplitude and low-field Hall feature are interrelated and originate from the suppression of the surface states' contribution to the conductivity by the magnetic field. Elevated Hall conductivity of the surface states may be either due to low concentration or due to an anomalous Hall effect. In our model, the Fermi level should be close to the Dirac point of the surface states. The magnetic field opens the Zeeman gap and suppresses the conductivity of the surface states and their contribution to the transport. This model qualitatively agrees with the data and, thus, is a candidate for the explanation of the observed features.

Nevertheless, the physical reason for the Hall nonlinearity and large WAL amplitude remains not firmly established. Our results, thus, draw the attention of theory and experiment to these phenomena.

II. SAMPLES AND EXPERIMENT

$Bi_{2-x}Sb_xTe_{3-y}Se_y$ (BSTS) films were grown by molecular beam epitaxy on a Si(111) substrate. The details of growth and structural characterization were described in Ref. [39]. Along with the compound $BiSbTeSe_2$ source, the elemental Bi and elemental Te sources were used. After obtaining the Si(111)-7 × 7 surface reconstruction, the sample was cooled to the growth temperature and kept at this temperature for one hour to reduce the surface temperature gradient on the sample. To passivate the silicon dangling bonds, which reduce the adatom diffusion length and lead to the quality degradation of the A^VB^{VI} compound growing layer, the tellurium source was opened for 3–5 minutes. The saturation of dangling bonds with tellurium atoms was evidenced by a decrease in the intensity of the Si(111)-7 × 7 surface structure. Then, a 2–4-nm-thick Bi_2Te_3 buffer layer was grown with the appearance of a continuous film being controlled by the emergence of a streaky reflection high-energy diffraction (RHEED) pattern. The substrate temperature T_{sub}, temperature of sources T_{Te}, T_{Bi}, and T_{BSTS}, and growth rate were changed (T_{sub} was between 345 and 370 °C, T_{BSTS} was 230-240 °C, and growth rate ν was changed in the range 0.07–0.5 nm/min) to find the optimal growth parameters. According to the atomic force microscopy data, the total $Bi_ySb_{2-y}Te_{3-x}Se_x$ film thickness is varied between 12 and 60 nm.

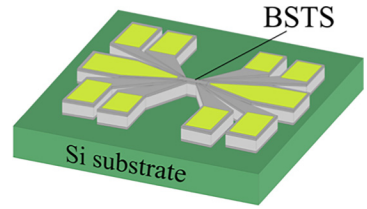

FIG. 1. Scheme of the structure with lithographically produced contacts. The gray color corresponds to the surfaces of BSTS; light gray corresponds to the BSTS bulk.

The structures for the transport measurements were prepared both by the shadow mask technique, where a standard six-terminal Hall bar mask was placed on top of a substrate, and by optical photolithography with HNO_3:CH_3COOH:H_2O_2:H_2O etchant being used to form a mesastructure on BSTS films. In the first case, indium contacts were sputtered atop; in the second one, Ti/Au contacts were defined with the lift-off technology.

Figure 1 shows a lithographically formed structure. Both In and Ti/Au contacts show the same transport characteristics. The magnetoresistance and temperature dependences of conductivity were measured in a helium Dewar in magnetic fields up to 4 T and also in the Oxford dry cryomagnetic system up to 12 T and temperature down to 1.64 K. The magnetic field was swept from positive to negative values and all magnetoresistance (Hall resistance) curves were symmetrized (antisymmetrized) to account for the misalignment of the potential contacts.

III. EXPERIMENTAL RESULTS

A. Observation of enhanced WAL prefactor

The temperature dependencies of the resistivity $R(T)$ for five samples under study (summarized in Table I) measured up to the liquid nitrogen temperature are shown in Fig. 2. [The typical $R(T)$ dependence measured to a higher temperature is given in the Supplemental Material [40] for sample 36; see Fig. S1]. For all samples, the resistance is weakly changed with temperature, i.e., not more than 5%, which indicates low carrier mobility and is rather general for 3D TI thin films. The nonmonotonic character of the temperature dependence is apparently due to the competition of several transport mechanisms: quantum corrections to conductivity, i.e., electron-electron correction and weak antilocalization, having different functional dependencies from bulk of the film and surface states, Fermi level drift, and phonon scattering. The low-temperature part of the $R(T)$ curve and the observed resistivity upturn at a temperature below 10–15 K are usually explained in a 3D TI by a collective contribution

TABLE I. Sample characteristics: film thickness d, mean free path l, parameters $\alpha_{\rm WAL}$, L_ϕ obtained from the fitting of the conductance data by Eq. (1), Hall concentration n_H, and mobility μ averaged in a 2–4 T magnetic-field Hall coefficient, measured at 4.2 K.

Sample	$\alpha_{\rm WAL}$	L_φ (nm)	$k_F \times l$	l (nm)	d (nm)	n_H ($\rm cm^{-2}$)	μ ($\rm cm^2/Vs$)
45	−1.01	58.2	7.8	10	12	9.4e12	200
46	−2.65	69.3	33	39	18	1.1e13	709
35	−1.19	72.2	9	9.7	14	1.3e13	159
36	−1.69	72.4	20.4	13.2	60	3.8e13	130
38	−3.11	81.3	34	16.5	35	6.9e13	121

of the WAL, weak localization (WL), and electron-electron interaction (EEI) corrections to the conductivity from the surface and bulk channels [14,41,42]. The low-temperature magnetoconductance (MC) for all films is similar and negative with a cusplike maximum at $B = 0$ (Fig. 3). Such behavior in TIs is usually associated with the suppression of the WAL correction to the conductivity of the surface states.

We fit the observed MC curves and $\Delta\sigma(B) = \sigma(B) - \sigma(0)$ in the conventional way [10] using the Hikami-Larkin-Nagaoka (HLN)-type formula,

$$\Delta\sigma(B) = \alpha\frac{e^2}{\pi h}\left[\Psi\left(\frac{B_0}{B}+\frac{1}{2}\right) - \ln\left(\frac{B_0}{B}\right)\right]. \qquad (1)$$

Here, $B_0 = \hbar/4e(L_\varphi)^2$, where L_φ is the phase coherence length, α is a constant that should be equal to $-1/2$ for WAL with one conducting channel, and $\Psi(x)$ is the digamma function.

An explicit comparison of the experimental results to the HLN theory is shown by the solid lines in Fig. 3. The experimental data for the perpendicular field MC are apparently well described by the WAL corrections, though the values of $\alpha_{\rm WAL}$ are unphysically large (see Table I). Our data are not surprising since the elevated values of $\alpha_{\rm WAL}$ were previously observed in a number of papers [2,13,16–20].

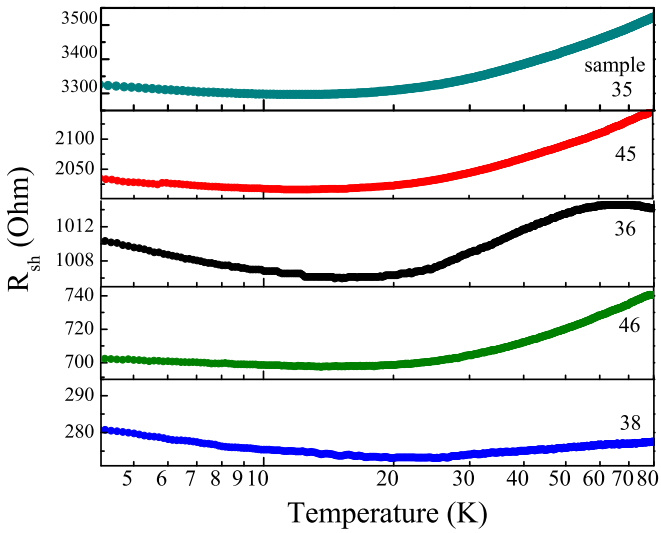

FIG. 2. Temperature dependence of resistance for different BSTS films.

It is often conjectured that an additional quadratic contribution to conductivity or linear magnetoresistance (LMR) due to macroscopic inhomogeneity of the film [21] may modify the prefactor [13,16,23,43]. We carefully checked numerically (see the Appendix) that it is not the case for our dataset: the $\alpha_{\rm WAL}$ value slightly modifies if the magnetoresistance is fitted by a sum of Eq. (1) and a parabolic or linear term. The elevated prefactor in Eq. (1) thus suggests an additional MC mechanism acting in parallel with WAL and leading to a sharp positive magnetoresistance.

B. High-field magnetoresistance. The role of electron-electron interaction correction

The high-field part of MC observed for all our samples as well as in some other studies [22,43,44] is not typical of WAL because the magnetic fields, in which the WAL effect must vanish, $B_{tr} \sim hc/el^2$, where l is a mean free path, should be less than 1 T.

Both the WL/WAL and macroscopic inhomogeneity mechanisms of magnetoresistance [21] are orbital effects and should be suppressed when the magnetic field is parallel to the TI film. To elucidate the nature of the high-field smooth $R(B)$ dependence with respect to the magnetic field, the sample rotation was carried out. As shown in Fig. 4 for samples 38 and 45 that have vastly different $\Delta\sigma$ and resistance values, the high-field part of magnetoresistance is weakly sensitive to the field direction. It means that the EEI corrections to the conductivity have to be taken into account. The EEI in the magnetic field must be affected by Zeeman splitting [45].

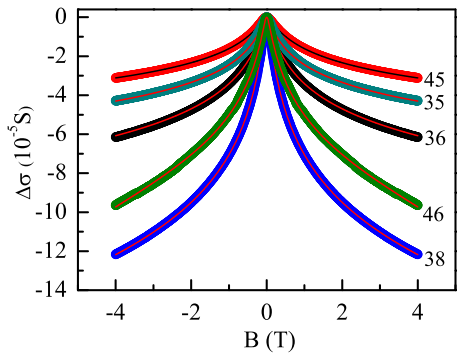

FIG. 3. Magnetoconductance $\Delta\sigma(B) = \sigma(B) - \sigma(0)$ of the samples under study in the magnetic field perpendicular to the sample plane, $T = 4.2$ K. Lines are the approximation with the HLN formula.

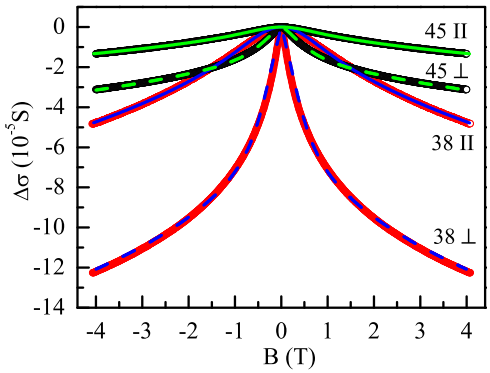

FIG. 4. Magnetoconductance $\Delta\sigma(B) = \sigma(B) - \sigma(0)$ for samples 45 and 38 in the magnetic field perpendicular and parallel to the sample plane, $T = 4.2$ K. Solid lines correspond to the EEI magnetoresistance; dashed lines correspond to the calculations with Eqs. (5)–(8) that include EEI, WAL, and the gap opening mechanism.

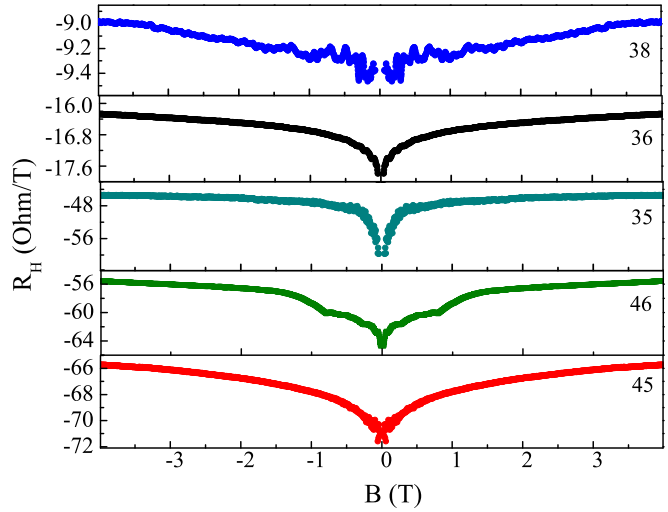

FIG. 5. Hall coefficients for the samples under study measured at 4.2 K.

This effect should be large enough due to the large g-factor, typically from 10 to 60 in tetradymite-based TIs [8,46–49].

Negative EEI magnetoconductance $\Delta\sigma_{\rm EEI}(B)$ appears when the spin splitting by an external field exceeds the temperature. In high magnetic fields ($g\mu_B B/k_B T \gg 1$), $\Delta\sigma_{\rm EEI}$ has a logarithmic-in-B dependence for 2D films and $\propto \sqrt{B}$ in the 3D case [50]. In arbitrary fields in 3D, it is described with the expression

$$\sigma_b(B) = \sigma_b^{(0)} - A_{\rm EEI} \times g_3\left(\frac{\mu_b g B}{T}\right). \qquad (2)$$

Here, $g_3(x) \propto \sqrt{x}$ for $x \gg 1$ is the dimensionless function. $A_{\rm EEI}$ is the amplitude of EEI magnetoresistance that depends on the diffusion coefficient in the bulk, the screening of Coulomb potential, and the film width. The g-factor may depend on the magnetic-field orientation (parallel or perpendicular to the film), but $A_{\rm EEI}$ cannot.

The 3D EEI mechanism reasonably agrees with the high-field part of the magnetoresistance data in a parallel magnetic field (solid lines in Fig. 4). The fitting parameters for sample 38 are $g_\parallel = 29.4$, $A_{\rm EEI} = 1.56 \times 10^{-5}$ S, and for sample 45, they are $g_\parallel = 35.6, A_{\rm EEI} = 0.38 \times 10^{-5}$ S. Here, $g_\parallel$ is the bulk g-factor in the parallel field. These values are in agreement with the typical g factors measured in tetradymite-based TIs [8,46–49]. We, thus, presume that the magnetoresistance in high perpendicular fields is also driven by EEI, and this correction originates from the bulk of the film.

In a perpendicular magnetic field, the orbital mechanisms of magnetoresistance should come into play. We showed that the magnetoresistance in very small perpendicular fields is described by WAL with an unphysically large prefactor $\alpha_{\rm WAL}$. Adding up EEI does not help to make the WAL amplitude reasonable. It means that besides WAL and EEI, there is an additional mechanism of magnetoconductance that is specific for our films. We believe that the key to the understanding of this mechanism is the Hall effect measurements described in the next section.

C. Low-field Hall nonlinearity

We measured the Hall resistance $R_{xy}(B)$ and focused on the Hall coefficient $R_H(B) \equiv R_{xy}(B)/B$. Figure 5 demonstrates the R_H(B) dependence for the samples under study measured at 4.2 K. One can see that the R_H dependence is nonlinear and strong in classically weak magnetic fields, $\lesssim 1$ T.

The scale of the effect differs from sample to sample. In the high carrier density of sample 38, there is almost no visible nonlinearity. However, the effect becomes essential in the lower density samples, where the TSSs do contribute to the conductivity.

In higher magnetic fields, the Hall coefficient smoothly continues to decrease, also in sample 38. This might be due to classical effects, such as two-liquid redistribution and field dependence of the mobility. In our paper, we focus on the low-field feature.

It is important that the effect does not demonstrate a visible temperature dependence in the low-temperature domain $T \lesssim 20$ K (see Fig. 6). It means that we may rule out most of the mechanisms suggested so far to explain the low-field Hall nonlinearity: WL-related current redistribution in inhomogeneous systems [38], second-order correction from WL/WAL

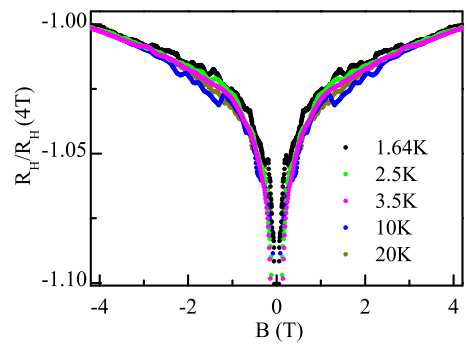

FIG. 6. Temperature dependence of Hall coefficients R_H for sample 36 normalized to the high-field R_H (4T) value.

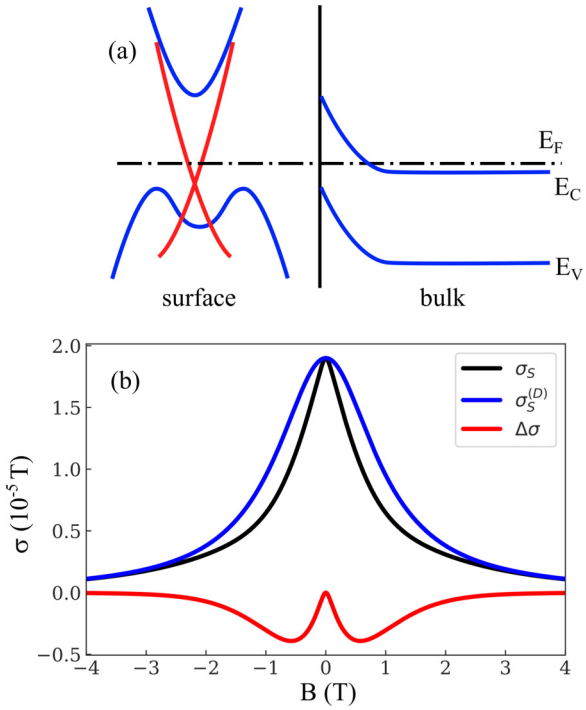

FIG. 7. Illustration of the model. (a) The energy spectrum of the bulk and surface states at zero magnetic field. (b) Drude surface conductivity $\sigma_s^{(D)}$, WAL correction $\Delta\sigma$, and the resulting surface conductivity σ_s for sample 45.

and EEI [30], and superconducting fluctuations [37]. In uniform systems, WL and WAL do not affect the Hall slope [28].

The absence of the temperature dependence along with the large value of the effect assume that its nature is related to the current flow redistribution: in elevated magnetic fields, the transport current bypasses the regions that strongly contribute to the Hall effect at a small magnetic field. It was natural to assume that low-field magnetoresistance, much exceeding the theoretical prediction, arises in only one component (e.g., topological surface states). A drop of its conductivity with the field, according to the two-liquid model, leads to a decrease of the fraction of the corresponding transport current. Since the TSSs had a low density, the overall Hall coefficient should decrease.

IV. MODEL

In this section, we show that both the elevated value of α and Hall nonlinearity can be explained within a model based on the following assumptions. (1) The chemical potential at the surface is close to the Dirac point. The surface electron concentration is small; the surface conductivity is of the order of the conductivity quantum [51,52]. The Hall conductivity of the surface in the magnetic field is high either within the Drude model or within the anomalous Hall mechanism [53]. (2) The chemical potential is inside the conductive band due to the strong band bending, shown in Fig. 7(a). The surface states are separated from the bulk with the tunnel barrier; therefore, the two kinds of states act as independent channels. (3) The second surface (Si-BSTS) does not contribute to the magnetoresistance and Hall effect (see Sec. V).

The surface states are described with the TI Hamiltonian

$$\hat{H} = v_0(\sigma_x p_y - \sigma_y p_x) + g_s \mu_B \boldsymbol{\sigma}\mathbf{B}. \tag{3}$$

Here, v_0 is the Fermi velocity at the Dirac point, $p_{x,y}$ is the surface electron momentum, and g_s is the surface electron g-factor that can be different from the g-factor in the bulk.

In a zero magnetic field, the surface states form a Dirac cone. We presume that the Fermi energy is shifted from the Dirac point by the small energy $\varepsilon_F^{(0)} \sim 10^{-2}$ eV, allowing the suppression of surface conductivity with a relatively low perpendicular magnetic field B_z that leads to the gap opening. The dispersion with finite B_z is as follows:

$$\varepsilon(p) = \pm\sqrt{v_0^2 p^2 + \varepsilon_Z^2}. \tag{4}$$

Here, $\varepsilon_Z = \mu_b g_s B_z/2$ is Zeeman energy in the perpendicular field. Note that the parallel field only shifts the Dirac point but does not open the gap, making the effect anisotropic.

The gap increases the effective mass and pushes the electrons towards the bulk states. This process is compensated by the apparent electric surface charge that results in the increase of the surface Fermi energy. When this compensation is strong, the 2D electron density is almost conserved and the Fermi energy is modified in the magnetic field [54],

$$\frac{\varepsilon_F}{\varepsilon_F^{(0)}} = \sqrt{1 + \left(\varepsilon_Z/\varepsilon_F^{(0)}\right)^2}. \tag{5}$$

Here we presume that the Zeeman energy is larger than the temperature.

The exact expression for the conductivity due to the emergence of electron mass depends on the particular scattering mechanisms. We consider the scattering by neutral impurities, which leads to the transport time $\tau_{tr} \propto \varepsilon_F^{-1}$. The Fermi mass $m \propto \varepsilon_F$ results in the Drude conductivity dependence on the Fermi energy,

$$\sigma_s^{(D)}(B) = \sigma_s^{(D)}(0)\frac{\varepsilon_F^2(0)}{\varepsilon_F^2(B)}. \tag{6}$$

We presume that the decrease of the Drude conductivity is responsible for the magnetoresistance in intermediate perpendicular fields, $B_z \sim 0.5$ T.

The spectrum modification also changes the WAL. In the low field, the WAL correction to the magnetoconductivity is significant due to sharp B dependence, $\sigma_s(B) = \sigma_s^{(D)}(B) + \Delta\sigma(B)$. $\Delta\sigma(B)$ is described by Eq. (1) with a single channel and $\alpha = -1/2$, which we do not treat as a fitting parameter.

The phase coherence length L_φ for the surface states is equal to $L_\varphi = \sqrt{D\tau_\varphi}$. Here, $D \sim v_F^2\tau_{tr}$ is the diffusion coefficient, τ_φ is the phase coherence time, and v_F is the Fermi velocity (which can be different from v_0 due to the gap opening). The EEI leads to $\tau_\varphi \approx \hbar^2 g(\varepsilon_F)D/T$ [45], where $g(\varepsilon_F)$ is the density of states at the Fermi level. Equation (1) is valid up to the transport field, $B_{tr} \sim \hbar^2/4eD\tau_{tr}$ [55].

Both D and $g(\varepsilon_F)$ are affected by the gap opening and increase of the apparent mass of surface electrons. It leads to the renormalization of B_0 in Eq. (1),

$$B_0(B) = B_0(0)\frac{\varepsilon_F(B)}{\varepsilon_F(0)}\left(1 - \frac{\varepsilon_Z^2}{\varepsilon_F^2(B)}\right)^{-2}. \tag{7}$$

Drude surface conductivity $\sigma_s^{(D)}(B)$, the WAL correction $\Delta\sigma$, and the total surface conductivity σ_s are shown in Fig. 7(b).

The sheet resistivity and the Hall coefficient are calculated within the two-liquid model (bulk with EEI and surface with WAL). Note that such model is valid when the bulk-surface scattering length is larger than the scattering length scales of the surface,

$$\sigma = \sigma_b + \sigma_s, \quad R_H = \frac{R_s\sigma_s^2 + R_v\sigma_v^2}{(\sigma_s + \sigma_v)^2}. \tag{8}$$

It shows that the sample conductivity σ is just the sum of σ_b and σ_s. The sample Hall coefficient R_H is some function of surface Hall coefficient R_s and bulk Hall coefficient R_b. It also depends on conductivities σ_b and σ_s.

Figure 4 shows the quantitative agreement between the perpendicular field magnetoconductance and the model including the EEI, WAL, and gap mechanisms (dashed lines). To achieve it, we first compared the high-field part of magnetoconductance with EEI [Eq. (2)], presuming that other mechanisms are saturated at $B \gtrsim 3$ T. In this analysis, the amplitude $A_{\rm EEI}$ was considered to be known from the parallel field magnetoconductance. We presume that the g-factor in perpendicular field $g_\perp$ differs from $g_\parallel$. The best agreement between the magnetoconductance measured in the high field and Eq. (2) is reached for $g_\perp = 39.4$ in sample 38 and $g_\perp = 56.9$ in sample 45. Then we compare the magnetoconductance in arbitrary fields with the two-liquid model. $\sigma_s(0)$, B_0, and $\varepsilon_F^{(0)}$ were considered as the fitting parameters. The dashed curves in Fig. 4 correspond to $\sigma_s(0) = 7.4 \times 10^{-5}$ S, $B_0 = 0.006$ T, $\varepsilon_F^{(0)}/\mu_b g_s = 0.6$ T for sample 38 and to $\sigma_s(0) = 1.75 \times 10^{-5}$ S, $B_0 = 0.035$ T, $\varepsilon_F^{(0)}/\mu_b g_s = 0.9$ T for sample 45. Note that in both samples, the surface conductance is comparable with $\sim e^2/h$.

The agreement between the experiment and Eq. (8) requires a rather small difference $\varepsilon_F^{(0)}$ between the Fermi level at the surface and the Dirac point. It should be comparable to the Zeeman energy in the field $\sim$1 T. With respect to a large g-factor $\sim$100, it corresponds to $\varepsilon_F^{(0)} \sim 0.01$ eV. Otherwise, if the Fermi level at the surface would lie far from the Dirac point, Eq. (6) results only in the correction to the conductivity that is quadratic over the magnetic field. It would be hardly distinguishable from the other mechanisms of quadratic magnetoconductance.

Figure 8 compares the Hall coefficient for samples 45 and 35 in the low magnetic field with the prediction of the model. From the magnetoconductance analysis, we get the following values for sample 35: $g_\perp = 48.14$, $\sigma_s(0) = 2.05 \times 10^{-5}$ S, $B_0 = 0.02$ T, $\varepsilon_F^{(0)}/\mu_b g_s = 0.5$ T. The values $R_s = -3220$ and $R_b = -68.3$ are used for fitting the Hall coefficient for sample 45 and $R_s = -5100$ and $R_b = -47.2$ for sample 35.

Note that the agreement between the experiment and the model requires R_s to be much larger than R_b. It corresponds to the assumption of low-surface-states' Fermi energy. The classical Hall coefficient is large for the small carrier density, while the anomalous Hall coefficient in TIs [53] is large for small Fermi energy $\varepsilon_F(0)$. Therefore, both mechanisms should lead to the anomalously strong contribution of surface transport to the Hall effect.

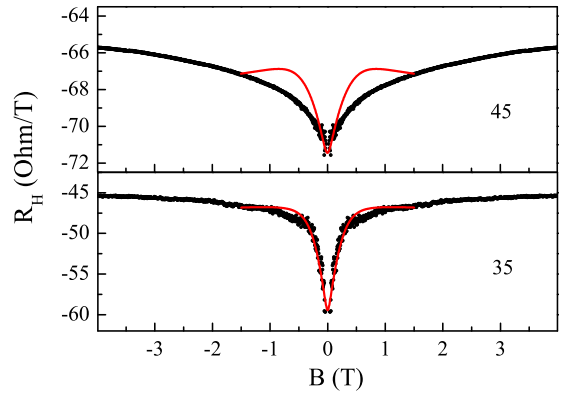

FIG. 8. Hall coefficient measured at 4.2 K for samples 35 and 45, compared with Eq. (8).

The qualitative agreement between experiment and model is shown in Fig. 8.

V. DISCUSSION

In our paper, we experimentally revealed a low-field Hall effect nonlinearity in 3D TI thin films. Our data differ from the previously reported observations of such nonlinearity in semiconducting 2D systems by a relatively large amplitude and weak temperature dependence. These signatures motivate us to believe that we deal not with coherent effects, but rather with the transport current redistribution due to the modification of the electron spectrum in the magnetic field. Namely, the system has several conductive components acting in parallel. The mobility of some of them (presumably Dirac surface states) drops with the magnetic field. At zero field, these states possessed a rather low density and high mobility and led to an elevated Hall constant. The magnetic field, therefore, promotes a drop of the Hall constant.

We note that besides the bulk, there are two surfaces in 3D TI thin films: top and bottom ones. These surfaces are not equivalent, which further complicates the problem. As a rule, the bottom surface is much more disordered due to the lattice mismatch and scattering [56]. An indirect indicator of different surfaces is the observation of WAL with prefactor $\alpha = 0.5$ instead of $\alpha = 1$ in most of 3D TI thin-film samples [12,18]. In some cases of well-adjusted 3D TI substrates, e.g., GaSe [57] or graphene [58], both surfaces contribute equally. We do not definitely know how many surfaces are effectively involved in our structures; however, we checked that for a qualitative comparison, the effective number of surface channels (1 or 2) is not essential.

Due to classically weak magnetic fields, we simplified the problem, neglected Landau quantization effects, and considered the theoretical effect of the Zeeman-field-induced gap opening for the Dirac states of 3D TI thin films. For realistic g-factor values ($\sim$50), this mechanism, along with WAL and EEI corrections, qualitatively explains much of the experimental data:

(1) The elevated value of the WAL prefactor $\alpha_{\rm WAL}$ obtained from the Hikami-Larkin-Nagaoka fit of low-field magnetoresistance. This value is high because the current redistribution contributes to positive magnetoresistance.

(2) Almost temperature-independent Hall nonlinearity driven by the spectrum modification and current redistribution.

(3) High-field monotonic magnetoresistance (almost the same in the parallel and perpendicular fields) due to electron-electron interactions.

The suggested mechanism involves a rough assumption of a specific surface band bending, so the Fermi level is close to the Dirac point. We cannot prove that it is indeed the case experimentally and cannot exclude that a more universal mechanism of the phenomenon will be found.

Note that the Hall nonlinearity is not usually reported. We believe there are two reasons for this: (i) researchers do not pay enough attention to the low-field limit for the Hall effect because they do not expect any nonlinearity and (ii) it is not easy to obtain thin films with a rather low carrier density, with the Fermi level close to the Dirac point for the topological surface states and, at the same time, with some bulk conduction electrons. For example, in Bi_2Te_3, the Dirac point is below the top of the valence band. In Bi_2Se_3, the Dirac point is in the middle of the 0.3 eV band gap, which is too far from the bottom of the conduction band. BSTS is probably ideal, therefore, for such observations.

Here, we should also discuss previous observations of an elevated WAL prefactor $\alpha_{\rm WAL} > 1$ in relation to our data. Recent work [17] reports $\alpha_{\rm WAL} \sim 1.4$ in BSTS microflakes, for the Fermi level close to the charge neutrality point (CNP). Away from the CNP, $\alpha_{\rm WAL}$ approached the theoretical value ~ -1. Similar behavior was observed in Ref. [2], where the authors studied the gate dependence of the conductivity and MR for the $(Bi_{0.57}Sb_{0.43})_2Te_3$ TI films around the Dirac point. These observations are in line with the mechanism suggested in our paper.

The elevated values of $\alpha_{\rm WAL}$ were also reported in Refs. [13,23,59,60]. Usually the observed values of $\alpha_{\rm WAL}$ and its temperature dependence are discussed in terms of several conductivity channels and their interaction. However, the most expected result of channel interaction is their merging, which would lead to the decrease of $\alpha_{\rm WAL}$ [61]; and $|\alpha_{\rm WAL}| > 1$ is hard to achieve with only two channels with WAL.

In Refs. [13,59], large values $|\alpha_{\rm WAL}| > 1$ appear only at elevated temperatures, while in Refs. [2,23], they are seen at low temperatures. In [23], $\alpha_{\rm WAL}(T)$ decreases with T. Our Eq. (6) is derived in the limit $T \ll \varepsilon_F(0)$; at larger temperatures, it should be suppressed. We do not think therefore that all the reports of elevated $\alpha_{\rm WAL}$ could be explained by a single physical mechanism. It is possible that our theory is related to the results of Refs. [2,23], but not Refs. [13,59]. We believe that the measurements of the Hall effect could be a useful tool to gain further insight.

The Hall nonlinearity in Bi_2Te_3 in magnetic fields $B \sim 1$ T was observed in Ref. [6] and attributed to the very high mobility of the surface states, $\mu \approx 10^4$ cm^2/Vs, which leads to $\mu B > 1$ already in low fields. For our low mobility films, this is definitely not the case. This assumption in our case would inevitably lead to very low Fermi energy and the importance of gap opening.

We believe that our paper will help to draw attention to the low-field domain and stimulate theory development and further experiments. In particular, the gap opening and current redistribution could be visualized by scanning probe techniques. Study of the Hall effect in gate-dependent measurements will also tell a lot about the effect because such measurements allow tuning the Fermi level at least for one of the surfaces.

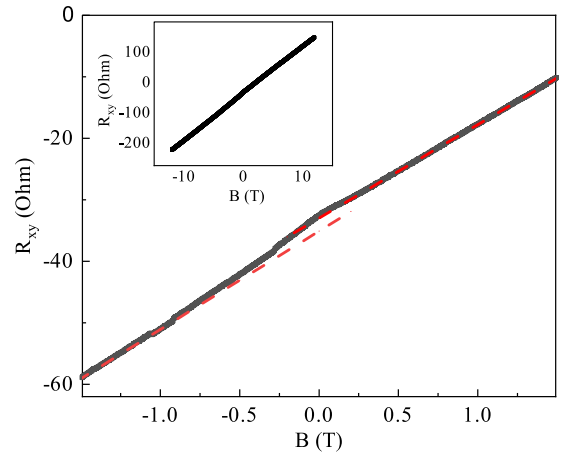

FIG. 9. Measured Hall resistance R_{xy}. Red dashed lines show asymptotics for high positive and negative fields. Inset shows R_{xy} in large magnetic fields.

VI. CONCLUSION

In this paper, we report on the anomalously large weak antilocalization and nonlinear Hall effect in thin films of BSTS 3D topological insulators. The Hall feature emerges in classically weak magnetic fields and weakly depends on the temperature. The existing theories fail to explain the observed phenomena. We suggest a possible mechanism of magnetoconductivity, related to the Zeeman-field-induced gap opening at the Dirac point, for the surface states in the perpendicular magnetic field. This gap decreases the conductivity of the surface states and, hence, their contribution to the Hall effect. Our mechanism qualitatively explains the observed phenomena, although the validity of the assumptions is yet to be confirmed.

ACKNOWLEDGMENTS

The authors are grateful to A. V. Nenashev for useful discussion. This work was supported by the Russian Science Foundation (Grant No. 22-22-20074) and Government of the Novosibirsk region.

APPENDIX A: HALL RESISTANCE

In Fig. 9, we present the raw data of the Hall resistance for sample 36 measured at $T = 1.64$ K, prior to the antisymmetrization procedure. The data contain an inevitable admixture of the diagonal component of the resistivity tensor, i.e., magnetoresistance, an even function of the magnetic field. The Hall coefficient is obtained by considering only the antisymmetric part of the data and its division over the magnetic field. Nevertheless, even from this dataset, it is easy to see that the Hall slope at $B = 0$ differs from the high-field asymptotics, which is a signature of the Hall anomaly at

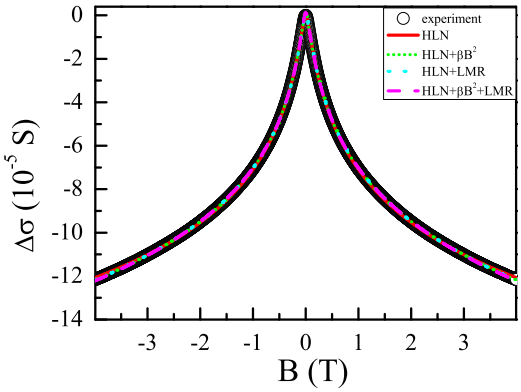

FIG. 10. Comparison of the magnetoresistance measured in sample 38 with Eq. (1) and Eqs. (B1)–(B3).

low field. The inset in Fig. 9 shows Hall resistance in a wide range of magnetic fields.

APPENDIX B: EFFECT OF QUADRATIC AND LMR CORRECTION TO HLN EXPRESSION

In the main text, we show that the measured magnetoconductivity is described by HLN formula (1) with unreasonably large α values. Sometimes [13,23], the elevated value of α in such a comparison is believed to be an artifact arising due to the quadratic contribution to magnetoconductivity $\delta\sigma \propto B^2$ or to linear magnetoresistance [21] $\delta R \propto |B|$. To rule out these explanations, we fit our magnetoconductivity data with the following expressions:

$$\Delta\sigma(B) = \beta B^2 + \alpha\frac{e^2}{\pi h}\left[\Psi\left(\frac{B_0}{B}+\frac{1}{2}\right) - \ln\left(\frac{B_0}{B}\right)\right], \quad \text{(B1)}$$

$$\Delta\sigma(B) = \frac{1}{R_0 + R'|B|} + \alpha\frac{e^2}{\pi h}\left[\Psi\left(\frac{B_0}{B}+\frac{1}{2}\right) - \ln\left(\frac{B_0}{B}\right)\right], \quad \text{(B2)}$$

TABLE II. Modifications of α and L_ϕ due to the quadratic and LMR contributions introduced in the model.

	HLN		HLN $+B^2$	
	α	L_φ (nm)	α	L_φ (nm)
35	−1.19	72.2	−1.15	76.3
36	−1.69	72.4	−1.35	72.4
38	−3.11	81.3	−3.04	83.05
45	−1.01	58.2	−1	59.7
46	−2.65	69.3	−2.47	71
	HLN+LMR		HLN+LMR+B^2	
	α	L_φ (nm)	α	L_φ (nm)
35	−1.18	72.5	−1.17	74.2
36	−1.72	69.7	−1.68	70.9
38	−2.71	90.4	−2.85	87.3
45	−0.86	65.7	−0.93	64.3
46	−1.63	96.3	−1.76	88.8

$$\Delta\sigma(B) = \beta B^2 + \frac{1}{R_0 + R'|B|} + \alpha\frac{e^2}{\pi h}\left[\Psi\left(\frac{B_0}{B}+\frac{1}{2}\right) - \ln\left(\frac{B_0}{B}\right)\right]. \quad \text{(B3)}$$

Here, Eq. (B1) corresponds to quadratic magnetoconductivity, Eq. (B2) to linear magnetoresistance, and Eq. (B3) includes both contributions. Figure 10 shows that all the equations can quantitatively describe the data. This result holds for all of our samples.

Table II shows the values of α_{WAL} and L_φ obtained from this fit with the least-squares method. Although α_{WAL} is actually slightly modified due to these contributions, it stays larger (in absolute value) than unity for all the samples besides 45. Approximation of MC was also made for the smaller magnetic fields (1.5 T) (not shown in Table II), but the α_{WAL} value had not changed much.

[1] W. Tian, W. Yu, J. Shi, and Y. Wang, Materials **10**, 814 (2017).
[2] M. Lang, L. He, X. Kou, P. Upadhyaya, Y. Fan, H. Chu *et al.*, Nano Lett. **13**, 48 (2013).
[3] M. Liu, C.-Z. Chang, Z. Zhang, Y. Zhang, W. Ruan, K. He, L. L. Wang, X. Chen, J.-F. Jia, S.-C. Zhang, Q.-K. Xue, X. Ma, and Y. Wang, Phys. Rev. B **83**, 165440 (2011).
[4] Y. Ando, J. Phys. Soc. Jpn. **82**, 102001 (2013).
[5] L. Zhang, M. Dolev, Q. I. Yang, R. H. Hammond, B. Zhou, A. Palevski, Y. Chen, and A. Kapitulnik, Phys. Rev. B **88**, 121103(R) (2013).
[6] D. X. Qu, Y. S. Hor, J. Xiong, R. J. Cava, and N. P. Ong, Science **329**, 821 (2010).
[7] Z. Ren, A. A. Taskin, S. Sasaki, K. Segawa, and Y. Ando, Phys. Rev. B **82**, 241306(R) (2010).
[8] A. A. Taskin, Z. Ren, S. Sasaki, K. Segawa, and Y. Ando, Phys. Rev. Lett. **107**, 016801 (2011).
[9] Y. Xu, I. Miotkowski, C. Liu, J. Tian, H. Nam, N. Alidoust, Jiuning Hu, C.-K. Shih, M. Z. Hasan, and Y. P. Chen, Nat. Phys. **10**, 956 (2014).
[10] S. Hikami, A. Larkin, and Y. Nagaoka, Prog. Theor. Phys. **63**, 707 (1980).
[11] M. Brahlek, N. Koirala, M. Salehi, N. Bansal, and S. Oh, Phys. Rev. Lett. **113**, 026801 (2014).
[12] R. Gracia-Abad, S. Sangiao, C. Bigi, S. K. Chaluvadi, P. Orgiani and J. María De Teresa, Nanomaterials **11**, 1077 (2021).
[13] B. A. Assaf, T. Cardinal, P. Wei, F. Katmis, J. S. Moodera, and D. Heiman, Appl. Phys. Lett. **102**, 012102 (2013).
[14] A. Y. Kuntsevich, A. A. Gabdullin, V. A. Prudkogliad, Y. G. Selivanov, E. G. Chizhevskii, and V. M. Pudalov, Phys. Rev. B **94**, 235401 (2016).
[15] L. Pandey, S. Husain, X. Chen, V. Barwal, S. Hait, N. K. Gupta, V. Mishra, A. Kumar, N. Sharma, N. Kumar, L. Saravanan, D. Dixit, B. Sanyal, and S. Chaudhary, Phys. Rev. Mater. **6**, 044203 (2022).
[16] Z. Wang, L. Yang, X. Zhao, Z. Zhang, and X. P. A. Gao, Nano Res. **8**, 2963 (2015).
[17] G. Shi, F. Gao, Z. Li, R. Zhang, I. Gornyi, D. Gutman, and Y. Li, Nat. Commun. **14**, 2596 (2023).

[18] J. Chen, X. Y. He, K. H. Wu, Z. Q. Ji, L. Lu, J. R. Shi, J. H. Smet, and Y. Q. Li, Phys. Rev. B **83**, 241304(R) (2011).

[19] J. G. Checkelsky, Y. S. Hor, M.-H. Liu, D.-X. Qu, R. J. Cava, and N. P. Ong, Phys. Rev. Lett. **103**, 246601 (2009).

[20] K. Shrestha, M. Chou, D. Graf, H. D. Yang, B. Lorenz, and C. W. Chu, Phys. Rev. B **95**, 195113 (2017).

[21] M. M. Parish and P. B. Littlewood, Nature (London) **426**, 162 (2003).

[22] S. Singh, R. K. Gopal, J. Sarkar, A. Pandey, B. G. Patel, and C. Mitra, J. Phys.: Condens. Matter **29**, 505601 (2017).

[23] N. K. Singh, D. Rawat, D. Dey, A. Elsukova, P. O. Å. Persson, P. Eklund, A. Taraphder, and A. Soni, Phys. Rev. B **105**, 045134 (2022).

[24] J. Lee, J. Park, J.-H. Lee, J. S. Kim, and H.-J. Lee, Phys. Rev. B **86**, 245321 (2012).

[25] N. H. Tu, Y. Tanabe, Y. Satake, K. K. Huynh, P. H. Le, S. Y. Matsushita, and K. Tanigaki, Nano Lett. **17**, 2354 (2017).

[26] B. Xia, P. Ren, A. Sulaev, P. Liu, S.-Q. Shen, and L. Wang, Phys. Rev. B **87**, 085442 (2013).

[27] Y. Xia, D. Qian, D. Hsieh, L. Wray, A. Pal, H. Lin, A. Bansil, D. Grauer, Y. S. Hor, R. J. Cava, and M. Z. Hasan, Nat. Phys. **5**, 398 (2009).

[28] H. Fukuyama, J. Phys. Soc. Jpn. **49**, 644 (1980).

[29] B. L. Altshuler, D. Khmel'nitzkii, A. I. Larkin, and P. A. Lee, Phys. Rev. B **22**, 5142 (1980).

[30] G. M. Minkov, A. V. Germanenko, O. E. Rut, A. A. Sherstobitov, and B. N. Zvonkov, Phys. Rev. B **82**, 035306 (2010).

[31] A. Y. Kuntsevich, L. A. Morgun, and V. M. Pudalov, Phys. Rev. B **87**, 205406 (2013).

[32] A. Joshua, S. Pecker, J. Ruhman, E. Altman, and S. Ilani, Nat. Commun. **3**, 1129 (2012).

[33] D. J. Newson, M. Pepper, E. Y. Hall, and G. Hill, J. Phys. C **20**, 4369 (1987).

[34] Y. Zhang, P. Dai, and M. P. Sarachik, Phys. Rev. B **45**, 6301 (1992).

[35] E. Tousson and Z. Ovadyahu, Phys. Rev. B **38**, 12290 (1988).

[36] A. P. Dmitriev and V. Y. Kachorovskii, Phys. Rev. B **77**, 193308 (2008).

[37] K. Michaeli, K. S. Tikhonov, and A. M. Finkel'stein, Phys. Rev. B **86**, 014515 (2012).

[38] A. Y. Kuntsevich, A. V. Shupletsov, and A. L. Rakhmanov, Phys. Rev. B **102**, 155426 (2020).

[39] N. P. Stepina, D. V. Ishchenko, V. A. Golyashov, A. O. Bazhenov, E. S. Goldyreva, I. O. Akhundov, A. S. Tarasov, K. A. Kokh, and O. E. Tereshchenko, Cryst. Growth Des. **22**, 7255 (2022).

[40] See Supplemental Material at http://link.aps.org/supplemental/10.1103/PhysRevB.108.115401 for the temperature dependence of the resistance of sample 36 measured up to high temperature.

[41] S. Sasmal, J. Mukherjee, D. Suri, and K. V. Raman, J. Phys.: Condens. Matter **33**, 465601 (2021).

[42] J. Wang, A. M. DaSilva, C. Z. Chang, K. He, J. K. Jain, N. Samarth, X. C. Ma, Q. K. Xue, and M. H. W. Chan, Phys. Rev. B **83**, 245438 (2011).

[43] G. M. Stephen, O. A. Vail, J. Lu, W. A. Beck, P. J. Taylor, and A. L. Friedman, Sci. Rep. **10**, 4845 (2020).

[44] S. X. Zhang, R. D. McDonald, A. Shekhter *et al.*, Appl. Phys. Lett. **101**, 202403 (2012).

[45] B. L. Altshuler and A. G. Aronov, Electron-electron interaction in disordered conductors, in *Modern Problems in Condensed Matter Sciences*, edited by A. L. Efros and M. Pollak (North-Holland Publising Company, Amsterdam, 1985).

[46] A. Wolos, S. Szyszko, A. Drabinska, M. Kaminska, S. G. Strzelecka, A. Hruban, A. Materna, M. Piersa, J. Borysiuk, K. Sobczak, and M. Konczykowski, Phys. Rev. B **93**, 155114 (2016).

[47] H. Köhler and E. Wöchner, Phys. Stat. Sol. B **67**, 665 (1975).

[48] J. G. Analytis, R. D. McDonald, S. C. Riggs, J.-H. Chu, G. S. Boebinger, and I. R. Fisher, Nat. Phys. **6**, 960 (2010).

[49] C.-X. Liu, X.-L. Qi, H. J. Zhang, X. Dai, Z. Fang, and S.-C. Zhang, Phys. Rev. B **82**, 045122 (2010).

[50] P. A. Lee and T. V. Ramakrishnan, Phys. Rev. B **26**, 4009 (1982).

[51] D. Culcer, E. H. Hwang, T. D. Stanescu, and S. Das Sarma, Phys. Rev. B **82**, 155457 (2010).

[52] R. S. Akzyanov and A. L. Rakhmanov, Phys. Rev. B **97**, 075421 (2018).

[53] N. A. Sinitsyn, A. H. MacDonald, T. Jungwirth, V. K. Dugaev, and J. Sinova, Phys. Rev. B **75**, 045315 (2007).

[54] A. Y. Kuntsevich, A. V. Shupletsov, and G. M. Minkov, Phys. Rev. B **97**, 195431 (2018).

[55] L. E. Golub, Phys. Rev. B **71**, 235310 (2005).

[56] J. Chen, H. J. Qin, F. Yang, J. Liu, T. Guan, F. M. Qu, G. H. Zhang, J. R. Shi, X. C. Xie, C. L. Yang, K. H. Wu, Y. Q. Li, and L. Lu, Phys. Rev. Lett. **105**, 176602 (2010).

[57] L. He, X. Kou, M. Lang, E. S. Choi, Y. Jiang, T. Nie, W. Jiang, Y. Fan, Y. Wang, F. Xiu, and K. L. Wang, Sci. Rep. **3**, 3406 (2013).

[58] N. P. Stepina, V. A. Golyashov, A. V. Nenashev, O. E. Tereshchenko, K. A. Kokh, V. V. Kirienko, E. S. Koptev, E. S. Goldyreva, M. G. Rybin, E. D. Obraztsova, and I. V. Antonova, Physica E **135**, 114969 (2022).

[59] P. Sahu, J.-Y. Chen, J. C. Myers, and J.-P. Wang, Appl. Phys. Lett. **112**, 122402 (2018).

[60] C. Shekhar, C. E. ViolBarbosa, B. Yan, S. Ouardi, W. Schnelle, G. H. Fecher, and C. Felser, Phys. Rev. B **90**, 165140 (2014).

[61] N. S. Averkiev, L. E. Golub, S. A. Tarasenko, and M. Willander, Phys. Rev. B **64**, 045405 (2001).